

Formation and accretion history of terrestrial planets from runaway growth through to late time : implications for orbital eccentricity

RYUJI MORISHIMA¹, MAX W. SCHMIDT

*Institute for Mineralogy and Petrography, Swiss Federal Institute of Technology,
Clausiusstrasse 25, 8092 Zurich, Switzerland*

Ryuji.Morishima@erdw.ethz.ch

and

JOACHIM STADEL, BEN MOORE

*Institute for theoretical physics, University of Zurich, Winterthurerstrasse 190, 8057
Zurich, Switzerland*

ABSTRACT

Remnant planetesimals might have played an important role in reducing the orbital eccentricities of the terrestrial planets after their formation via giant impacts. However, the population and the size distribution of remnant planetesimals during and after the giant impact stage are unknown, because simulations of planetary accretion in the runaway growth and giant impact stages have been conducted independently. Here we report results of direct N-body simulations of the formation of terrestrial planets beginning with a compact planetesimal disk. The initial planetesimal disk has a total mass and angular momentum as observed for the terrestrial planets, and we vary the width (0.3 and 0.5AU) and the number of planetesimals (1000-5000). This initial configuration generally gives rise to three final planets of similar size, and sometimes a fourth small planet forms near the location of Mars. Since a sufficient number of planetesimals remains, even after the giant impact phase, the final orbital eccentricities are as small as those of the Earth and Venus.

Subject headings: Accretion, terrestrial planets

¹The office is at Institute for theoretical physics, University of Zurich, Winterthurerstrasse 190, 8057 Zurich, Switzerland

1. Introduction

The rocky planets are believed to have formed via the accretion of small planetesimals. The formation mechanism of planetesimals and their initial mass and spatial distribution are however still controversial. The standard picture of accretion of terrestrial planets from planetesimals is as follows. During the early stages of planetesimal accretion, larger planetesimals grow faster than smaller ones owing to their stronger gravity (Greenberg et al. 1978; Wetherill & Stewart 1989). Through this runaway growth stage, a few tens of Mars-size protoplanets form with mutual separation of 10 Hill radii (Kokubo & Ida 1998, 2002). The growth time scale of protoplanets is estimated to be $\sim 0.1\text{--}1\text{Myr}$ around 1AU, and is longer with larger distance from the Sun (Wetherill & Stewart 1993; Kokubo & Ida 2002). As long as some amount of nebular gas and/or planetesimals remain, its damping effect stabilizes the orbits of protoplanets, preventing mutual collisions (Iwasaki et al. 2002; Kominami & Ida 2002). As the amount of remnant gas and/or planetesimals decreases, the orbital eccentricities of protoplanets increases due to their mutual interactions. Eventually their orbits become chaotic and late time giant impacts occur. During this giant impact stage, whose time scale is considered to be $\sim 100\text{Myr}$, the current terrestrial planets form (e.g. Chambers & Wetherill 1998; Agnor et al. 1999; Kokubo et al. 2006). The orbital eccentricities of planets immediately after giant impacts are likely to be much larger than those of the current terrestrial planets. Therefore, interactions with remnant gas and/or planetesimals is expected to reduce their eccentricities. Reviews for the processes described above are given by Chambers (2004); Nagasawa et al. (2007).

Whether remnant gas or remnant planetesimals is more important for reducing eccentricities primarily depends on the time scale of gas dissipation. If the time scale is long, the velocity dispersion of planetesimals is suppressed by the gas drag. Hence, the gravitational focusing effect of protoplanets is enhanced, resulting in a fast clean up of remnant planetesimals and a lower eccentricity distribution of the final planets (Agnor & Ward 2002; Kominami & Ida 2002, 2004; Nagasawa et al. 2005; Ogihara et al. 2007). On the other hand, if the time scale of gas dissipation is short, planetesimals remain unaccreted by protoplanets for a longer period of time. In this case, remnant planetesimals may be required to reduce the eccentricities (Chambers 2001; O’Brien et al. 2006; Raymond et al. 2006). In this paper, we examine the latter scenario. In other words, we ignore the effects of the gas drag and the tidal interaction between a gas disk and protoplanets. The effects of gas will be investigated in a future study.

There have been several attempts to examine the effect of remnant planetesimals based on direct N -body simulations (Chambers 2001; O’Brien et al. 2006; Raymond et al. 2006), and with simulations using a hybrid-code (Kenyon & Bromley 2006). Direct N -body simu-

lations usually adopt lunar to Mars size protoplanets surrounded by smaller planetesimals as initial conditions. Direct N -body simulations suggest that the eccentricities of final planets are further reduced as the total mass of planetesimals increases. Even for the same total mass of planetesimals, the damping effect is stronger with a larger number of smaller planetesimals (O’Brien et al. 2006; Raymond et al. 2006). However, the total mass and mass distribution of the remaining planetesimals are unknown, unless mass evolution in the runaway stage is followed.

The hybrid code of Kenyon & Bromley (2006); Bromley & Kenyon (2006), is able to follow planetary accretion through both the runaway and giant impact stages. In their code, the mass and velocity distributions of planetesimals contained in multi annuli are solved by a statistical approach whereas orbits of protoplanets are solved using direct N -body calculations, that include the effect of interaction between planetesimals and protoplanets. Statistical approaches based on the local approximation produce consistent results with those obtained from direct N -body simulations in the runaway stage (e.g. Inaba et al. 2001). However, it is questionable if statistical approaches can accurately follow the late stage of planetary accretion because orbital eccentricities of remnant planetesimals are usually very large.

Here we report results of direct N -body simulations beginning with a planetesimal disk until the end of planetary accretion in the terrestrial region. We consider compact planetesimal disks (initial disk widths of $\leq 0.5\text{AU}$), whose total masses and total angular momenta are the same as those of the present terrestrial planets. These initial conditions are used since accretion simulations beginning from compact disks are usually computationally less expensive than those from wider disks. This is the case even with the same initial number of particles, because of the rapid decrease in the number of particles through accretion. Another reason to adopt compact disks is that total angular momenta of final planetary systems obtained from most of previous simulations are much larger than for the terrestrial planets, as these simulations usually have a super-massive Mars (e.g. Chambers 2001; Raymond et al. 2006). This excess angular momentum is likely due to initially extended disks. Though Jupiter removes angular momentum, mostly from the asteroid region, its effect does not seem to be sufficiently strong in the terrestrial region. As one possibility for this issue, we consider initially compact disks, supposing that they result from, for example, dust migration due to the gas drag prior to formation of planetesimals (e.g. Youdin & Shu 2002).

In § 2, we explain the numerical methods used in this study. We show results of simulations in § 3. We compare our results with previous simulations in § 4. In § 5, we give some physical interpretations for our simulation results using analytic estimations. We summarize our results in § 6.

2. Methods

The runaway growth stage is shorter than the giant impact stage, but orbits of a large number of bodies need to be followed. On the other hand, although fewer bodies are necessary for the giant impact stage (unless the effect of fragmentation is considered), more care must be taken to accurately follow the orbital evolution over many more dynamical times. Taking these physically different types of the accretion stages into account, we apply different N -body codes to these two stages of the evolution.

The runaway growth stage is simulated with the parallel tree-code *PKDGRAV* (Richardson et al. 2000; Stadel 2001) for 10^5 yr with adopting artificially enhanced radii. The code uses a fourth-order multi-pole expansion for the force calculations, and a second-order leap-frog scheme is used for time integration. We apply a hierarchical time stepping with the largest time step of 1.8 days (0.005 yr). The opening angle of 0.5 is used as a criterion for searching down the tree. The energy error in the runaway stage is $|\Delta E/E| \sim 10^{-4}$ – 10^{-3} , arising entirely from the integrator. The error due to the force calculation using our tree method is negligibly small. Using the output of the runaway stage as the initial condition, we simulate the giant impact stage with the hybrid symplectic code *Mercury* (Chambers 1999) for 2×10^8 yr without any enhancement of radii. This code uses a mixed variable symplectic (MVS) method (Kinoshita et al. 1991; Wisdom & Holman 1991; Saha & Tremaine 1992) for orbits around the Sun whereas close encounters are integrated by the Bulirsch-Stoer method. We use a fixed time step of 6 days, which is the same as or similar to those adopted in the previous works using *Mercury* (Chambers 2001; Raymond et al. 2006). The energy error in the giant impact stage is $|\Delta E/E| \sim 10^{-5}$. It usually takes less than one computer day for a simulation of the runaway stage with *PKDGRAV*, whereas it can take several months to compute the giant impact stage with *Mercury*.

Whereas MVS type integrators can take much larger time steps than those used with the leap-frog scheme, the *Mercury* code uses direct summation for calculations of the mutual gravity force. *PKDGRAV* is thus faster than *Mercury* as long as the number of particles is larger than several hundred. Some comparisons between these two codes are also found in Raymond (2005).

The enhancement of radii in the runaway stage is used in order to reduce computational time; we use an enhancement factor of radii $g = 4.3$. This gives an analogous effect of the gas drag, and the growth time scale of protoplanets is reduced by a factor of $\sim g^2$ (Kokubo & Ida 1996, 2002, see also eq. [20]). On the other hand, the growth time scale of protoplanets is actually reduced by a factor of $\sim \beta^2$ by the gas drag, where β is the factor for reduction of planetesimal eccentricities (Kokubo & Ida 2000). Thus, our simulations approximately mimic a situation in which the gas disappears suddenly at $(g/\beta)^2 \times 10^5$ yr. This time scale is

probably shorter than the typical life time of circumstellar disks, \sim a few Myr (Haisch et al. 2001), although the exact time scale for formation of planetesimals from dusty gaseous disks is not known. As long as the number of planetesimals is sufficient, the orbits of protoplanets are stabilized during the runaway stage by dynamical friction such that the growth mode is not affected by the enhancement of radii (Kokubo & Ida 1996). However, in the transition from the runaway growth stage to the giant impact stage, faster clean up of remnant planetesimals, due to this approach, usually causes final planets to have higher eccentricities. Thus the radii of particles should be set to realistic values before planetesimals are too depleted in order to accurately examine the effect of remnant planetesimals. Additional simulations and analytic calculations were performed to assess the sensitivity of the results to varying the time at which g is reduced to unity.

We use 10 different initial conditions which are summarized in Table 1. The total mass and angular momentum are assumed to be the same as for the present terrestrial planets ($1.98M_E$ and $1.86M_E \text{ AU}^{1/2} \sqrt{GM_\odot}$, respectively, where M_E , G , and M_\odot stand for the mass of Earth, the gravitational constant, and the solar mass, respectively) with the central star’s mass equal to the solar mass. The initial width of a planetesimals disk Δ_{disk} is taken to be 0.3 AU or 0.5AU. The planetesimal mass is assumed to be identical and the number of planetesimals N varies from 1000 to 5000. The physical density of all the bodies is assumed to be $\rho = 2 \text{ g cm}^{-3}$. The surface number density $n(a)$ as a function of the semimajor axis a is given by a power law $n(a) \propto a^\alpha$ with $\alpha = -1$ or -2 . We also conduct two additional simulations for $N = 1000$, where we switch the code and g at $5 \times 10^4 \text{ yr}$ in order to check whether the outcomes are affected by this timing.

It would be very interesting to investigate the accretion of planets using more extended disks ($\Delta_{\text{disk}} > 0.5\text{AU}$), but computationally too expensive with our current codes. The rate at which planetesimals merge is slower in a wider disk, particularly at its extremities, so we need to use the tree method for the gravity calculation for longer period of time. On the other hand, it is not appropriate to use the leap-frog integrator for the long-term orbital evolution for the following reasons. Firstly, since the leap-frog integrator causes a secular error in the longitude of the perihelion (Kokubo & Makino 2004), it does not accurately treat long-term secular interactions. Secondly, since the standard (or explicit) block multi-timestep algorithm used for the leap-frog integrator is not time-symmetric, the error in the energy accumulates with close encounters (Hut et al. 1995). This is also the case for the higher order Hermite-integrator (Kokubo & Makino 2004). We ensure that the transition from *PKDGRAV* is chosen conservatively, thus we achieve high energy conservation as mentioned above.

Although the implicit block time-step algorithm can avoid this problem (Makino et al.

2006), MVS integrators have considerable advantages for simulations of planetary accretion. We are therefore implementing the SyMBA integrator (Duncan et al. 1998) into the latest version of *PKDGRAV*, which enables us to simulate planetary accretion in wider disks. These simulation results will be reported later.

3. Results

3.1. An example of evolution: Run 6

As an example, we first explain time evolution of Run 6. For this simulation the width of the initial disk Δ_{disk} is 0.5AU and the initial number of planetesimals N is 3000. Figure 1–3 show time evolution of this simulation: snapshots on the plane of the semimajor axis versus the orbital eccentricity (Fig. 1), the cumulative number of planetesimals plotted against the mass (Fig. 2), and the epicyclic velocity plotted against the mass (Fig. 3). For detailed analysis, we divide the accretional evolution into four different stages (the runaway, oligarchic, giant impact, and post giant impact stages), rather than two main stages discussed so far.

3.1.1. Runaway growth stage ($\sim 10^4$ yr)

In the early stage, most of the mass of the system is contained in smallest planetesimals. In this case the epicyclic velocity, $v = \langle a\Omega\sqrt{e^2 + i^2} \rangle$ (where Ω is the orbital frequency, and e and i are the orbital eccentricity and inclination of a planetesimal, respectively), is regulated by the smallest planetesimals and is typically as large as their escape velocity; $v_{\text{esc},0} = \sqrt{2Gm_0/(gr_0)}$ (Fig. 3), where m_0 and r_0 are the mass and the radius. If v is much smaller than the escape velocity of the largest body $v_{\text{esc},p} = \sqrt{2Gm_p/(gr_p)}$ (where m_p and r_p are the mass and the radius respectively), and is a decreasing function with mass as shown in Figure 3, then the largest body starts to grow much faster than nearby objects. This growth mode is called runaway growth (Wetherill & Stewart 1989; Kokubo & Ida 1996; Weidenschilling et al. 1997). At $t \sim 10^4$ yr, the power-law index q ($dN_c \propto m^q dm$, where N_c is the cumulative number and m is the planetesimal mass) is about -2.7 in our simulation (Fig. 2). This value is close to $q \simeq -2.5$ obtained in simulations of Kokubo & Ida (1996, 2000) and the analytical estimate $q = -8/3$ by Makino et al. (1998). (Makino et al. (1998) assumed complete energy partitioning ($v \propto m^{-1/2}$) in the strong gravitational limit ($v \ll v_{\text{esc},0}$). However, the actual velocity distribution is less steep than this (Rafikov 2003, see also our Fig. 3). If we assume $v \propto m^\gamma$ with $\gamma \sim -1/4$, which is a rough approximation of Figure 3 at $t \sim 10^4$ yr, the formulation of Makino et al. (1998) gives $q = -13/6 + \gamma \sim -2.4$.)

3.1.2. Oligarchic growth stage ($\sim 10^5$ yr)

As large bodies grow, their mutual gravitational interactions leave their orbits separated by 5–10 Hill radius (Kokubo & Ida 1995, 1998, see also our Fig. 5). The Hill radius r_H of a planetesimal of mass m_p is given by

$$r_H = ah_p = a \left(\frac{2m_p}{3M_\odot} \right)^{1/3}, \quad (1)$$

where a is its semimajor axis and h_p is the reduced Hill radius. The largest bodies gravitationally influence the velocity evolution of all the neighboring planetesimals (Ida & Makino 1993), increasing towards the escape velocity of the protoplanet $v_{\text{esc,p}}$ (see the panel of $t = 10^5$ yr in Fig. 3). On the other hand, the velocities of protoplanets v_p are also influenced by the energy partitioning with surrounding smaller planetesimals. Indeed, the value of v_p for Run 6 is quite close to the equilibrium value $v_{p,\text{eq}}$ ($\sim v_{\text{esc},0}$), which is theoretically estimated neglecting the mutual perturbations of protoplanets (see eq. [35] in § 5.3).

Since the growth rate of the largest body slows down at the expense of its nearby neighbors, the largest intermediate mass objects begin catch up with the largest body (Ida & Makino 1993). This growth mode is called oligarchic growth (Kokubo & Ida 1998). At $t = 10^5$ yr in Run 6, about half of the total mass is contained in the 10 largest oligarchic bodies. Since the growth of smaller planetesimals has substantially stalled, protoplanets start to separate from the continuous size distribution. Therefore, the number of planetesimals decreases mostly by accretion onto protoplanets and not by mutual collisions. Since v for planetesimals is nearly independent of the mass, so is their collision probability with protoplanets. Hence, the power-law index q for the mass distribution of planetesimals does not change from -2 after this stage.

3.1.3. Giant impact stage ($\sim 10^6$ yr)

Without the damping force by remnant planetesimals and/or gas, a multiple protoplanet system undergoes an orbital instability after a certain time T_{inst} . This instability time T_{inst} depends on the orbital separation, eccentricities, and absolute mass of protoplanets (Chambers et al. 1996; Ito & Tanikawa 1999; Yoshinaga et al. 1999; Iwasaki & Ohtsuki 2006). We switch the code and reduce the value of g from 4.3 to 1 at $t = 10^5$ yr. For Run 6, T_{inst} this time is estimated to be 10^5 – 10^6 yr from above studies. With a decreasing total mass of planetesimals that have higher velocities, the damping due to the dynamical friction of planetesimals becomes less effective. At this point the orbital instability and mutual collisions of protoplanets start to take place. We find that the orbital instability starts

immediately after $t = 10^5$ yr, and the number of protoplanets decreases from 12 at $t = 10^5$ yr to 10 at $t = 2 \times 10^5$ yr (here we assume a protoplanet to be a body with mass $> 2 \times 10^{26}$ g $\sim 50m_0$).

During the giant impact stage, the mass distribution changes mainly owing to collisions between protoplanets, while the population of small planetesimals does not change so much. This can be seen in Figure 2; from $t = 10^5$ yr to $t = 10^6$ yr, when the number of protoplanets reduces from 12 to 5, whereas the total number of particles reduces only from ~ 400 to ~ 300 . Because the velocities of protoplanets are much smaller than those of planetesimals, mutual collisions of protoplanets occur quickly. This is similar to results of simulations including the damping force due to the tidal interaction between a gas disk and protoplanets; Kominami & Ida (2002) find that the giant impact stage becomes shorter with the stronger damping force.

3.1.4. *Post giant impact stage ($> 10^7$ yr)*

The number of protoplanets further reduces to 3 at $t = 10^7$ yr, after two final giant impacts that occur shortly before $t = 10^7$ yr. Through the giant impact stage, the mutual separation between protoplanets normalized by their Hill radii increases to ~ 30 . The mass distribution becomes completely bimodal (Fig. 2) with the masses of protoplanets smaller than the isolation mass by a factor of ~ 3 . The isolation mass is the total mass contained in a ring of width 30 Hill radius with the initial surface density (see eq. [19]). This deviation likely comes from decrease of the surface density (by a factor of ~ 2) due to expansion of the disk from its initial diameter via gravitational scattering of protoplanets. For remnant planetesimals, the power-law index q remains to be ~ -2 and the largest mass is $\sim 50m_0$, which is similar to the protoplanet’s mass during the runaway to oligarchic stages.

Since the mutual interactions between protoplanets after the giant impact stage is rather weak, the eccentricities of protoplanets are expected to be determined by the energy partitioning with remnant planetesimals. As we discussed for the oligarchic stage, v_p in the giant impact phase is surprisingly close to the equilibrium value ($\simeq v_{\text{esc},0}$; see eq. [35]), although some amount of remnant planetesimals may be necessary to achieve full equilibrium. For this simulation we find that the fraction of the total mass contained in planetesimals is 0.29 and 0.16 at $t = 10^6$ and 10^7 yr, respectively. Naively, one might predict that equilibrium occurs once the mass in planetesimals is comparable to the total mass of protoplanets (see § 5.2). This slight contradiction might mean that the damping due to giant impacts themselves or some other unknown mechanism, works effectively.

3.2. Evolution of orbital spacing and eccentricities

Here we analyze the evolution of each simulation quantitatively and discuss its dependence on the initial conditions. In order to examine characteristics of the evolution of the largest bodies, we define a planet (or a protoplanet) as a body having mass larger than 2×10^{26} g. The physical meaning of this choice is that a body larger than this mass regulates the velocity evolution of all the neighboring bodies (see § 5.3). In this case the following discussion does not strongly depend on the definition of the minimum mass of planets. We will explore the following four quantities: [1] the number of planets, N_p , [2] the mass fraction of planets compared to the total mass, f_p , [3] the orbital spacing of planets normalized by the mutual Hill radius, \bar{b}_p , [4] the eccentricity of planets, \bar{e}_p , and [5] the ratio of the effective mass of planetesimals to the mean mass of protoplanets $m_{\text{eff}}/\langle m_p \rangle$. The effective mass of planetesimals is defined as $m_{\text{eff}} = \langle m^2 \rangle / \langle m \rangle$, where $\langle m^2 \rangle$ and $\langle m \rangle$ are the mean squared and mean masses of planetesimals, whose masses are smaller than 2×10^{26} g. The mass ratio $m_{\text{eff}}/\langle m_p \rangle$ would be important for the evolution of \bar{e}_p , as its equilibrium value due to the dynamical friction is given by (eq. [15] in § 5.1)

$$e_{p,\text{eq}} \simeq \sqrt{\frac{4m_{\text{eff}}}{3\langle m_p \rangle}} \langle e^2 \rangle^{1/2}. \quad (2)$$

We apply the following form for the averaged orbital spacing normalized by the mutual Hill radius

$$\bar{b}_p = \sqrt{\frac{\sum_{j=1}^{N_p-1} ((a_{j+1} - a_j)/r_{H,j})^2 \mu_j}{\sum_{j=1}^{N_p-1} \mu_j}}, \quad (3)$$

with the reduced mass

$$\mu_j = \frac{m_{p,j} m_{p,j+1}}{m_{p,j} + m_{p,j+1}}, \quad (4)$$

and the mutual hill radius

$$r_{H,j} = \frac{1}{2}(a_j + a_{j+1}) \left(\frac{m_{p,j} + m_{p,j+1}}{3M} \right)^{1/3}. \quad (5)$$

Here a_j , e_j , and $m_{p,j}$ are the semimajor axis, orbital eccentricity, and mass of the protoplanet j in the order of semimajor axis, respectively. We use the following form for the averaged eccentricity, which characterizes the energy of epicyclic motion of planets:

$$\bar{e}_p = \sqrt{\frac{\sum_{j=1}^{N_p} m_{p,j} e_j^2}{\sum_{j=1}^{N_p} m_{p,j}}}, \quad (6)$$

where e_j is the orbital eccentricity of the protoplanet j . The mass weighted eccentricity (e.g. Bromley & Kenyon 2006; Raymond et al. 2006) gives a slightly smaller value than the above eccentricity.

Figure 4 shows the evolution of these four quantities for the case of $\Delta_{\text{disk}} = 0.3\text{AU}$. In the third panel from the top, we also plot the orbital instability time as a function of the orbital spacing for the two cases of $\bar{e}_p/\bar{h}_p = 2$ and 4, respectively, from Yoshinaga et al. (1999) (see eq. [26]). Here $\bar{h}_p = (2\langle m_p \rangle / (3M_\odot))^{1/3}$ is the averaged reduced hill radius. These lines indicate the stability of multiple protoplanet systems; if the orbital spacing is narrower than these lines, orbital instability will occur. Several protoplanets form at $\sim 10^4$ yr and the normalized orbital spacing \bar{b}_p is about 10, as pointed out by Kokubo & Ida (1998). Since the orbital instability time is 10^5 – 10^6 yr in such systems, giant impacts between protoplanets start around that time as we discussed in the previous section. The orbital eccentricity prior to the giant impact stage is ~ 0.03 while it increases up to 0.1 during the giant impact stage. The corresponding normalized eccentricities, \bar{e}_p/\bar{h}_p , are 2–3 and ~ 10 , respectively. Through the giant impact stage, \bar{b}_p increases to 20–30. As the radial excursion of planets during the giant impact stage determines the final separation of planets, the relation between \bar{b}_p in the final state and \bar{e}_p during the giant impact stage can be approximately represented by (Kominami & Ida 2002)

$$\bar{b}_p \bar{h}_p \sim 2\bar{e}_p. \quad (7)$$

This is roughly consistent with our simulation results.

During the post giant impact stage, the orbital eccentricities are reduced ($\bar{e}_p/\bar{h}_p \sim 3$) and these values have little dependence on initial parameters (we discuss the weak dependence in detail in § 5.3). Since \bar{b}_p is large enough in the final state, the mutual interaction of planets is likely to be unimportant. In this case, final eccentricities of planets are expected to be determined by the energy partitioning with remnant planetesimals. The mass ratio $m_{\text{eff}}/\langle m_p \rangle$ decreases nearly monotonically with time and is about 0.01–0.02 in the final state (the bottom panel of Fig. 4; the decrease of $m_{\text{eff}}/\langle m_p \rangle$ is due to the increase of $\langle m_p \rangle$, while m_{eff} is nearly constant except at very early times). Since the mean eccentricity of planetesimals is ~ 0.3 in the post giant impact stage (Fig. 3), the equilibrium eccentricity of planets (eq. [2]) is estimated to be 0.03–0.05. This is almost the same as the values obtained in our simulations.

While the final giant impact occurs before $t \sim 10^7$ yr in most of the runs, it happens at $t \sim 5 \times 10^7$ yr for Run 1 ($N = 1000$). Because of that impact, the orbital spacing for Run 1 becomes even wider. This unstable behavior likely suggests that the dynamical friction for $N = 1000$ is less effective as compared with larger N . However, except for this event, the dependence of the evolutions of all the quantities shown in Figure 4 on N is very

small. Switching g in the earlier time does not affect the quantities in the final state shown in Figure 4, either, although Run 1b is dynamically more excited during the giant impact stage. This is because the mass variation of protoplanets in Run 1b is somewhat large and smaller protoplanets are dynamically enhanced by larger protoplanets.

Figure 5 is the same as Figure 4, but for the case of $\Delta_{\text{disk}} = 0.5\text{AU}$. The evolution of all the quantities are very similar to those in Figure 4, although the early evolution is slightly slower due to the lower initial surface density. The dependence on N is very small here as well as in Figure 4. In particular, the final \bar{b}_p has converged to ~ 30 for all the runs. However, the final eccentricity \bar{e}_p is much larger for the case with earlier switching of g (Run 5b). This is in an opposite sense to our prediction because dynamical friction works more effectively with a higher density of planetesimals. We will discuss this issue in the next section along with the final configurations of the systems. Except for Run 5b, \bar{e}_p and $m_{\text{eff}}/\langle m_p \rangle$ in Figure 5 are slightly smaller than those in Figure 4. The smaller m_{eff} is due to the smaller surface density (the relation is roughly given by $m_{\text{eff}} \propto \Sigma^{3/2}$, where Σ is the initial surface density of planetesimals; see § 5.3).

3.3. Final systems

Here we present the orbital parameters of all the final systems obtained in our simulations. Figure 6 shows snapshots of all of our runs on the a - e plane at 200Myr. Also, the number of planets N_p , the averaged eccentricities of planets \bar{e}_p , and the angular momentum deficit of planetary systems S_d at 200Myr are summarized in Table 1. The angular momentum deficit is defined as (Laskar 1997; Chambers 2001)

$$S_d = \frac{\sum_{j=1}^{N_p} m_{p,j} \sqrt{a_j} \left(1 - \sqrt{(1 - e_j^2) \cos i_j}\right)}{\sum_{j=1}^{N_p} m_{p,j} \sqrt{a_j}}, \quad (8)$$

where i_j is the orbital inclination of the planet j . We take 5Myr averages for \bar{e}_p and S_d . For the current terrestrial planets, we take the mean values between the minimum and maximum orbital eccentricities and inclinations from 3Myr orbital integrations in Quinn et al. (1991). This operation roughly corresponds to subtracting only the free eccentricities, provided that the free eccentricities is larger than the forced eccentricities due to giant planets (see Murray & Dermott 1999, Chap. 7.4). In fact, the minimum eccentricities and inclinations obtained in Quinn et al. (1991) are almost zero except for Mercury. This suggests that the free eccentricity (inclination) and the forced eccentricity (inclination) are comparable for the current terrestrial planets.

We always obtain three similar size planets between 0.5AU and 1.3 AU, except Run 1 has

only two planets in this region. The orbital spacing between planets are also quite similar. We find that more than 95% of the initial mass and angular momentum are contained in planets at 200Myr in all our simulations. Both the averaged eccentricities and the angular momentum deficits obtained from our simulations are comparable or even smaller than those for the current solar system, except for Run 5b and Run 8 (Table 1). Except these two runs, both \bar{e}_p and S_d are smaller for $\Delta_{\text{disk}} = 0.5\text{AU}$ than for $\Delta_{\text{disk}} = 0.3\text{AU}$. There seems to be a weak tendency that \bar{e}_p and S_d decrease with increasing N . These trends are interpreted in terms of the effective planetesimal mass m_{eff} , if the final \bar{e}_p is determined by the energy partitioning with planetesimals neglecting the mutual interaction of planets (§ 5.3).

Differing from other runs, the mutual interaction between the innermost two planets in Run 5b and Run 8 is important even at the end of simulations, as their orbital separation is narrow. This seems related to the spatial distribution of planetesimals during the giant impact stage. In these runs, we find that two innermost planets quickly sweep out planetesimals in the inner region whilst there are still large numbers of planetesimals in the outer region. The outer planets with these planetesimals tend to push the middle planet inward. As a result, the two innermost planets continue interacting without sufficient dynamical friction due to surrounding planetesimals. Although our statistics is not sufficient, such a difference in the inner and outer region would tend to appear when g is reduced at earlier times or if the initial planetesimal mass were concentrated in the inner region.

This fact seems related to the existence of the small outermost planet. When we compare simulations Run 1 and Run 1b, the sizes and locations of two largest planets are very similar. While Run 1b has inner and outer small planets, Run 1 has only an outer small planet (near 2.1AU). Similarly, while the sizes and locations of the three largest planets in Run 5 and Run 5b are similar, only Run 5b has an outermost planet. These facts suggest that the tendency to have small planets in the inner and outer edges is stronger in simulations with earlier switching of g . We interpret this as due to a larger amount of planetesimals that are scattered inward (outward) at the inner (outer) edge of the disk before they are accreted by planets. Small planets form from these scattered planetesimals. A similar trend is also found in the simulations starting with a stronger gradient of the surface density in the radial direction (Runs 4 and 8). In these systems, the inner planets form quickly while large planets have not grown in the outer region. Then inner planets gravitationally scatter planetesimals and small protoplanets outward. The orbital eccentricities of protoplanets scattered outward are reduced by the dynamical friction of similarly scattered planetesimals. Eventually, these protoplanets can have stable orbits near the location of Mars and slightly grow as they collide with planetesimals.

4. Comparison with previous works

Our simulation results are different from those starting with only protoplanets. Kokubo et al. (2006) conducted simulations starting with ~ 15 mars-size protoplanets at $0.5 < a < 1.5\text{AU}$ and found that most of the final mass is contained in the largest two planets. Their final orbital eccentricities are usually higher than those for the current terrestrial planets. Chambers & Wetherill (1998) also showed similar results to Kokubo et al. (2006) for the case without perturbation of Jovian planets (their Model A). They also found that mass concentration within fewer planets is strengthened by the presence of Jovian planets (their Model B). The difference between their results and ours suggests that the number of final planets increases with a stronger damping force, which makes the radial excursion of protoplanets and thus the final separation between neighboring planets narrower. Indeed, the same trend was also found by Kominami & Ida (2002), who examined the effect of damping due to the gas disk on the accretion of protoplanets.

In recent direct N -body simulations starting with planetary embryos with small planetesimals, the total mass of planetesimals is half or less than half, and the orbital separation of embryos is equal to or less than 10 in units of the Hill radii (Chambers 2001; O’Brien et al. 2006; Raymond et al. 2006). Since the dynamical friction of surrounding planetesimals is not strong enough to suppress the orbital instability with these initial conditions (see § 5.2), giant impacts start immediately before planets substantially grow by accretion. They adopt a nearly identical size distribution of planetesimals, which in principle, does not change in such enhanced systems. Therefore, the effective mass of planetesimals after giant impacts occur is still given by the initial planetesimal mass. Thus, the dependence of the equilibrium eccentricity of planets on the initial planetesimal mass ($e_{p,\text{eq}} \sim \sqrt{m_0/\langle m_p \rangle} \langle e^2 \rangle^{1/2}$) is much stronger than we find. In some of their simulations, mutual interaction amongst the final planets is insignificant and the final eccentricities seem to be close to the equilibrium value. For example, O’Brien et al. (2006) adopt the initial mass of planetesimals to be $m_0 \simeq 1/400M_E$. In the late stages of their EJS (eccentric orbits of Jupiter and Saturn) simulations, most of the mass supplied to terrestrial planets is from small planetesimals with very high speed. If we convert their impact speed $\sim 20\text{km s}^{-1}$ in the late stage to the eccentricity around 1AU, it gives $\langle e^2 \rangle^{1/2} \sim 0.5$. Supposing that the mean mass of planets is as large as the Earth’s mass, we obtain $e_{p,\text{eq}} \sim 0.025$, which is even smaller than those for the current terrestrial planets, and consistent with their results. Therefore, we predict that the final eccentricities of planets would be further reduced if they adopted smaller planetesimal masses in their simulations. However, such a small effective mass of planetesimals in the beginning of the giant impact stage might be unlikely if we take the growth of planetesimals in the runaway and oligarchic stages into account.

Kenyon & Bromley (2006) and Bromley & Kenyon (2006) conducted planetary accretion simulations starting with very small planetesimals ($r_0 = 1\text{--}5\text{km}$), using their hybrid code. In their runs, simulations starting at 0.86–1.16AU in Kenyon & Bromley (2006) have similar initial conditions to ours, although our disks are slightly more massive. The evolution of the number of oligarchic bodies (with masses $>\sim 10^{25}\text{--}10^{26}\text{g}$ in their simulations) and their orbital separation (their Hill parameter almost corresponds to $1/\bar{b}_p$) are very similar to our results. However, the final eccentricities of planets is more excited in their simulations (one of their simulations obtained three planets with $e_p \sim 0.1$). In fact, in all of their simulations starting with wider initial disks (0.4–2.0AU), the final planetary orbits are more eccentric than the current terrestrial planets (see Table I of Kenyon & Bromley 2006), and apparently remnant small planetesimals do not contribute to damping of eccentricities of planets. Since we have not conducted simulations starting with wide disks, it is not clear for us if their results obtained with a hybrid code are consistent with those obtained from direct N -body simulations. We are planning to conduct direct N -body simulations with initially wide disks to clarify this problem.

5. Analytic estimates

In this section, we interpret our simulation results using analytic estimates.

5.1. Evolution of velocities of planetesimals and protoplanets

First we provide analytic formulation for the evolution of velocities of planetesimals and protoplanets necessary for subsequent discussions. Consider a situation in which protoplanets are spatially separated but mutually interact due to the distant perturbations and each protoplanet is surrounded by a swarm of planetesimals. We first consider equal-mass planetesimals, then the formulation is extended to the case of continuous size distribution (protoplanets are always assumed to be equal-mass). The mass, mean square eccentricity, and surface number density of planetesimals are represented as m , $\langle e^2 \rangle$, and n , respectively. Corresponding characters for protoplanets are m_p , $\langle e_p^2 \rangle$, and n_p , respectively. The scattering cross section for planetesimal-planetesimal encounters $\sigma_{\text{sca}}^{m-m'}$ and that for protoplanet-planetesimal encounters $\sigma_{\text{sca}}^{m_p-m'}$ are given by (Ida & Makino 1993)

$$\sigma_{\text{sca}}^{m-m'} = C_e \left(\frac{G(m+m')}{(a\Omega)^2(\langle e^2 \rangle + \langle e'^2 \rangle)} \right)^2, \quad (9)$$

$$\sigma_{\text{sca}}^{m_{\text{p}}-m'} = C_e \left(\frac{G(m_{\text{p}} + m')}{(a\Omega)^2(\langle e_{\text{p}}^2 \rangle + \langle e'^2 \rangle)} \right)^2, \quad (10)$$

where C_e is the numerical factor of ~ 40 , G is the gravitational constant, a is the distance of the system from the Sun, and Ω is the orbital frequency. In equation (9), we used primed characters, m' and $\langle e'^2 \rangle$, to distinguish two interacting planetesimal groups (the primed values are averaged later). Using the scattering cross sections, the change rates of $\langle e^2 \rangle$ and $\langle e_{\text{p}}^2 \rangle$ are given by

$$\begin{aligned} \frac{1}{\Omega} \frac{\langle e^2 \rangle}{dt} &= n \left(\frac{m'}{m + m'} \right)^2 \sigma_{\text{sca}}^{m-m'} (\langle e^2 \rangle + \langle e'^2 \rangle) + n_{\text{p}} \left(\frac{m_{\text{p}}}{m_{\text{p}} + m} \right)^2 \sigma_{\text{sca}}^{m_{\text{p}}-m} (\langle e_{\text{p}}^2 \rangle + \langle e^2 \rangle) \\ &= C_e \left(\frac{G}{(a\Omega)^2} \right)^2 \left(\frac{nm'^2}{\langle e^2 \rangle + \langle e'^2 \rangle} + \frac{n_{\text{p}}m_{\text{p}}^2}{\langle e_{\text{p}}^2 \rangle + \langle e^2 \rangle} \right), \end{aligned} \quad (11)$$

$$\frac{1}{\Omega} \frac{\langle e_{\text{p}}^2 \rangle}{dt} = \left(\frac{1}{m_{\text{p}} + m'} \right)^2 (4nm'^2 \langle e'^2 \rangle - 3nm'm_{\text{p}} \langle e_{\text{p}}^2 \rangle + nm'^2 \langle e_{\text{p}}^2 \rangle) \sigma_{\text{sca}}^{m_{\text{p}}-m'} + \frac{\langle e_{\text{p}}^2 \rangle}{\Omega T_{\text{Inst}}}, \quad (12)$$

where T_{Inst} is the time scale for orbital instability of protoplanets (see § 5.2). In equation (11), the first term stands for the viscous stirring due to planetesimal-planetesimal encounters while the second term for the viscous stirring due to protoplanet-planetesimal encounters (Ida & Makino 1993). In equation (12), the first term stands for the sum of viscous stirring and the dynamical friction both due to encounters with planetesimals (Ida & Makino 1992) while the second term approximately accounts for the enhancement due to distant interactions between protoplanets. The rate of change of the inclinations are given by similar equations, but here we omit them.

The surface number density per unit mass is given by dn/dm . As in the simplest case, we assume that $\langle e'^2 \rangle$ is independent of mass. In this case, after integration of equations (11) and (12) over the range of m' , nm' and nm'^2 in these equations can be replaced by

$$\int m' dn, = \Sigma_{\text{s}}, \quad \int m'^2 dn = \Sigma_{\text{s}} m_{\text{eff}}, \quad (13)$$

respectively. Here Σ_{s} and $m_{\text{eff}} = \langle m'^2 \rangle / \langle m' \rangle$ are the surface density and effective mass of planetesimals, respectively. Using these averaged quantities, we have simple implications from equations (11) and (12). Equation (11) suggests that the velocity evolution of planetesimals is regulated by protoplanet-planetesimal encounters rather than by planetesimal-planetesimal encounters if

$$n_{\text{p}} m_{\text{p}}^2 > f_e \Sigma_{\text{s}} m_{\text{eff}}, \quad (14)$$

where $f_e \leq 1$ is the numerical factor associated with the velocity distribution. Equation (12) suggests that the eccentricity of planets is given by

$$\langle e_{\text{p,eq}}^2 \rangle = \frac{4m_{\text{eff}}}{3m_{\text{p}} - m_{\text{eff}}} \langle e^2 \rangle, \quad (15)$$

in the equilibrium state provided that the mutual interaction between protoplanets is negligible.

During the giant impact stage, in which orbits of protoplanets cross each other, the second term in the right hand side of equation (12) can be replaced by the mutual viscous stirring term:

$$\left(\frac{1}{\Omega} \frac{\langle e_p^2 \rangle}{dt}\right)_{\text{mut}} = \frac{1}{2} \sigma_{\text{sca}}^{m_p - m_p} \langle e_p^2 \rangle, \quad (16)$$

with the cross section for the mutual scattering

$$\sigma_{\text{sca}}^{m_p - m_p} = C_e \left(\frac{Gm_p}{(a\Omega)^2 \langle e_p^2 \rangle} \right)^2. \quad (17)$$

The averaged eccentricity of protoplanets during the giant impact stage is determined by the balance between the mutual viscous stirring and the dynamical friction due to surrounding planetesimals. Assuming $m_p \gg m_{\text{eff}}$ and $m_p \langle e_p^2 \rangle \gg m_{\text{eff}} \langle e^2 \rangle$, we obtain

$$\langle e_p^2 \rangle_{\text{GI}}^{1/2} = \left(\frac{1}{6} \frac{n_p m_p}{\Sigma_s} \right)^{1/4} \langle e^2 \rangle^{1/2}. \quad (18)$$

The same expression is obtained in Goldreich et al. (2004) except for a factor of order unity. Equation (18) somewhat overestimates $\langle e_p^2 \rangle^{1/2}$ during the giant impact stage as compared with those obtained from our simulations. This is probably because the motion of all the planets are not enhanced simultaneously in our simulations as some planets are in stable orbits isolated from others.

5.2. Comparison of time scales and timing of the onset of giant impacts

Here we discuss how the timing of the onset of the giant impact stage is affected by the radius enhancement factor g . Since the time and distance can be rescaled for our N -body simulations, g is physically associated with the ratio of the physical radius r to the Hill radius r_H as $g \propto r/r_H \propto a^{-1} \rho^{-1/3}$.

For simplicity in this section, we call the most massive body in its feeding zone of width of $b_p r_H$, a planet (note that the definition of planets used in the main text follows the discussion in § 5.3). Defining the mass ratio of the planet with the total mass in the feeding zone to be f_p , the planet mass m_p is given as

$$\begin{aligned} m_p &= 2\pi f_p a b_p r_H \Sigma = (2\pi f_p b_p \Sigma)^{3/2} a^3 (2/3 M_\odot)^{1/2} \\ &\simeq 0.06 \left(\frac{b_p}{10}\right)^{3/2} \left(\frac{\Sigma}{20 \text{ g cm}^{-2}}\right)^{3/2} \left(\frac{f_p}{0.25}\right)^{3/2} \left(\frac{a}{1 \text{ AU}}\right)^3 M_E, \end{aligned} \quad (19)$$

where Σ is the surface density of all the bodies (thus assumed to be constant regardless of f_p). For $f_p = 1$, m_p corresponds to the so-called isolation mass (e.g. Kokubo & Ida 2000).

Considering a two component system composed of planets and surrounding planetesimals, we introduce the following five timescales, which characterize the evolution of planets and surrounding planetesimals. [1] The growth time scale of planet T_{grow} is given by

$$T_{\text{grow}} = \left| \frac{1}{m_p} \frac{dm_p}{dt} \right|^{-1} = \frac{m_p}{(1 - f_p)\Sigma\sigma_{\text{col}}\Omega}, \quad (20)$$

with the collisional cross section σ_{col} (Greenzweig & Lissauer 1992):

$$\sigma_{\text{col}} = c_{\text{col}}(gr_p)^2 \left(\frac{1}{3} + \frac{1}{\tilde{v}^2} \right), \quad (21)$$

where c_{col} is a numerical factor of ~ 8 (we assume $\langle e^2 \rangle^{1/2} = 2\langle i^2 \rangle^{1/2}$) and \tilde{v} is the averaged velocity of planetesimals normalized by the escape velocity of the planet. [2] The depletion time scale of planetesimals T_{dep} is given by

$$T_{\text{dep}} = \left| \frac{1}{(1 - f_p)\Sigma} \frac{d(n_p m_p)}{dt} \right|^{-1} = \frac{m_p}{f_p \Sigma \sigma_{\text{col}} \Omega}, \quad (22)$$

where $n_p = f_p \Sigma / m_p$ is the surface number density of planets. [3] The time scale for the evolution of the velocity of planetesimals T_{sca} due to gravitational scattering by planets is given by

$$T_{\text{sca}} = \left| \frac{1}{\langle e^2 \rangle} \frac{d\langle e^2 \rangle}{dt} \right|^{-1} = \frac{m_p}{f_p \Sigma \sigma_{\text{sca}} \Omega}. \quad (23)$$

Here the scattering cross section σ_{sca} corresponds to $\sigma_{\text{sca}}^{m_p - m'}$ (eq. [10]) in the limit of $m_p \gg m'$ and $\langle e_p^2 \rangle \ll \langle e'^2 \rangle$

$$\sigma_{\text{sca}} = c_{\text{sca}}(gr_p)^2 \frac{1}{\tilde{v}^4}, \quad (24)$$

where c_{sca} is a numerical factor of ~ 16 . Note that σ_{sca} does not directly depend on g . However, as the velocity can be scaled by the escape velocity of the planet, which depends on g , σ_{sca} indirectly depends on g as represented by equation (24). [4] The time scale for damping the velocity of planets T_{damp} due to dynamical friction of surrounding planetesimals is given by

$$T_{\text{damp}} = \left| \frac{1}{\langle e_p^2 \rangle} \frac{d\langle e_p^2 \rangle}{dt} \right|^{-1} = \frac{m_p}{(1 - f_p)\Sigma\sigma_{\text{sca}}\Omega}. \quad (25)$$

[5] The time scale for the orbital instability T_{inst} of a multiple protoplanetary system without any damping force represents either the time of the first collision or the first close

encounter (see Yoshinaga et al. 1999, for comparison of T_{inst} with different types of definitions). The form of T_{inst} is empirically given by (Chambers et al. 1996; Yoshinaga et al. 1999; Ito & Tanikawa 1999; Iwasaki & Ohtsuki 2006)

$$\log \left(\frac{T_{\text{inst}}}{T_{\text{orb},1}} \right) = c_1 b_p + c_2, \quad (26)$$

where $T_{\text{orb},1}$ is the orbital period of the innermost protoplanet, and c_1 and c_2 are numerical coefficients. These coefficients depend strongly on the orbital eccentricity and relatively weakly on the absolute averaged mass and the variation of masses. The dependence of c_1 and c_2 on orbital eccentricities is summarized in Table III of Yoshinaga et al. (1999). For $b_p = 10$ and $\bar{e}_p \sim 4\bar{h}_p$, $T_{\text{inst}}/T_{\text{orb},1} \sim 10^5 - 10^6$.

For simplicity, we normalize all the timescales as follows:

$$\tilde{T} = \frac{c_{\text{col}} \Sigma (g r_p)^2}{m_p} \Omega T. \quad (27)$$

With this normalization, all the time scales except for \tilde{T}_{inst} depend only on \tilde{v} and f_p as

$$\begin{aligned} \tilde{T}_{\text{grow}}^{-1} &= (1 - f_p) \left(\frac{1}{3} + \frac{1}{\tilde{v}^2} \right), \\ \tilde{T}_{\text{dep}}^{-1} &= f_p \left(\frac{1}{3} + \frac{1}{\tilde{v}^2} \right), \\ \tilde{T}_{\text{sca}}^{-1} &= 2f_p \frac{1}{\tilde{v}^4}, \\ \tilde{T}_{\text{damp}}^{-1} &= 2(1 - f_p) \frac{1}{\tilde{v}^4}. \end{aligned} \quad (28)$$

It should be noted that now the dependence on g is included only in \tilde{T}_{inst} .

In order to obtain the time scales as functions of f_p , we consider the evolution of \tilde{v} . In the early stages the smallest planetesimals dominate the mass of the system so that the velocity is as large as the escape velocity of planetesimals. The exact value of \tilde{v} at the initial state (when $m_p = m_0$) is determined by the balance between the mutual scattering and the collisional damping. Since the ratio of these time scales is given by the ratio of σ_{col} to σ_{sca} , we obtain $\tilde{v} = 1.17$ for the initial state. Since the dimensional velocity of planets is $1.17v_{\text{esc},0}$, \tilde{v} decreases as planets grow (or with increasing f_p). When f_p reaches to a certain value, planets start to regulate the velocities of surrounding planetesimals. In this case, \tilde{v} evolves as planets grow. Thus, \tilde{v} is obtained from $\tilde{T}_{\text{grow}} = \tilde{T}_{\text{sca}}$ (Daisaka et al. 2006). The value of \tilde{v} increases with f_p to 1.17 at $f_p = 0.5$. For $f_p > 0.5$, \tilde{T}_{dep} becomes shorter than \tilde{T}_{sca} , if $\tilde{v} > 1.17$. This means that planetesimals collide with planets before their velocities are further enhanced. Therefore, \tilde{v} takes a constant value, 1.17, for $f_p > 0.5$.

We plot the evolution of \tilde{v} as a function of f_p in Figure 7. In the same figure, we also plot \tilde{T}_{grow} , \tilde{T}_{sca} , \tilde{T}_{damp} , and \tilde{T}_{inst} with the parameters used in Run 6 and $b_p = 10$. For \tilde{T}_{inst} , we take $T_{\text{inst}}/T_{\text{orb}} = 5 \times 10^5$ with $g = 1$ and 4.3 as examples. This time scale would be appropriate judging from our simulations. It should be noted that $\tilde{T}_{\text{dep}} = \tilde{T}_{\text{sca}}$ for $f_p > 0.5$ and \tilde{T}_{dep} further increases with decreasing f_p for $f_p \leq 0.5$, although we do not plot \tilde{T}_{dep} on Figure 7 in order to avoid confusion due to too many lines.

Iwasaki et al. (2002) and Iwasaki & Ohtsuki (2006) showed that orbital instability is prevented when $\tilde{T}_{\text{damp}} < c_3 \tilde{T}_{\text{inst}}$, with a coefficient c_3 of the order of unity (we assume $c_3 = 3$ after Iwasaki & Ohtsuki (2006)). Hence, the value of f_p at the onset of giant impacts is estimated from the equation $\tilde{T}_{\text{damp}} = 3\tilde{T}_{\text{inst}}$, and is 0.3–0.4 and 0.8–0.9 for $g = 1$ and 4.3, respectively, in Figure 7. However, Figure 7 also suggests that $\tilde{T}_{\text{inst}}(g = 4.3) > \tilde{T}_{\text{dep}}$, which means that remnant planetesimals are depleted before the giant impact phase starts, as long as we keep $g = 4.3$. Complete depletion of planetesimals keeping $b_p \sim 10$ is found in simulations with $g = 6$ in Kokubo & Ida (2002) and Leinhardt & Richardson (2005), and we also found the same results with additional tests. Therefore, in order to keep some amount of planetesimals at the onset of the giant impact stage, it must start before f_p reaches 0.5 (strictly speaking, this value is slightly higher than 0.5 for $c_3 > 1$). This also corresponds to the condition for the damping of enhanced eccentricities of planets during the giant impact stage. The condition under which the eccentricities of planets are damped before depletion of planetesimals is given by $\tilde{T}_{\text{damp}} < \tilde{T}_{\text{dep}}$, which gives $f_p < 0.5$ (Fig. 7). For the case of $g = 1$, this condition is satisfied. The threshold value of g to satisfy the condition is roughly estimated to be 3.

For our simulations (except Runs 1b and 5b), we reduced g from 4.3 to 1 when f_p is about 0.6 (Figs. 4 and 5). After reducing g , \tilde{T}_{inst} becomes smaller than any other timescale (Fig. 7). Thus, the giant impact phase rapidly begins (the instantaneous reduction of g causes drop of \tilde{v} to $\sim 1.17/\sqrt{4.3}$, but \tilde{T}_{sca} is shorter than \tilde{T}_{grow} by a factor of 4.3 with this small \tilde{v} and thus \tilde{v} increases near to 1.17 again before f_p substantially increases). On the other hand, for Runs 1b and 5b, f_p is about 0.4 when we reduce g at 5×10^4 yr. In these cases giant impacts do not start immediately as $\tilde{T}_{\text{damp}} \sim 3\tilde{T}_{\text{inst}}$ at $f_p \sim 0.4$ (this can be seen in Figs. 4 and 5 as N_p does not change immediately after reducing g). In fact, after f_p increases to ~ 0.5 , giant impacts start in these simulations. Therefore, it is expected that reducing g at an earlier time does not affect the results (we have now conducted some simulations keeping fixed $g = 1$ and obtained consistent results; these results will be reported in another paper).

To summarize, for simulations with a constant g throughout the entire accretion stage, sweeping up all the planetesimals and a subsequent giant impact stage are expected for

$g > 3$, whereas giant impacts during accretion of planetesimals and a subsequent damping of eccentricities of planets due to the dynamical friction are expected for $g < 3$. For $g < 3$, the evolution and final state of a system are expected to weakly depend on g , from the comparison between Runs 1 and 1b and that between Runs 5 and 5b.

5.3. Minimum oligarchic mass and equilibrium eccentricity of protoplanets

Once the mass of the largest body is above a certain critical mass, the velocity evolution of neighboring planetesimals is primarily regulated by the largest body. We call this critical mass the minimum oligarchic mass. Then, the growth of smaller planetesimals near the largest body is stalled and as the largest body grows it starts to separate from the continuous size distribution of planetesimals. Therefore, the planetesimal size distribution after this stage is expected to be a continuous distribution with the maximum mass being the minimum oligarchic mass. This size distribution determines the equilibrium eccentricity of planets after the giant impact stage. Here we estimate the planetesimal size distribution, when the largest body starts to regulate the velocity evolution of all of its neighboring planetesimals.

We consider the power-law size distribution for planetesimals $dn \propto m^q dm$ with the upper and lower cutoff masses m_p and m_0 . The condition that the largest body regulates the velocity evolution is again given by (eq. [14])

$$m_p^2 > f_e m_T m_{\text{eff}}, \quad (29)$$

where f_e is a factor associated with the velocity distribution and is slightly smaller than unity and $m_T (= \Sigma_s/n_p)$ is the total mass of planetesimals (excluding the largest body or a planet) in the heated region, where velocities are regulated by a planet (see Ida & Makino 1993), with n_p being the surface number density of planets (the sizes of the heated region and the feeding zones are similar). We also define the cumulative number in the heated region to be $N_h = n/n_p$, and now the size distribution is given by $dN_h = km^q dm$. Using the condition for the mass of the largest planetesimals (or the second largest body in the heated region) m_L

$$2 = \int_{m_L}^{\infty} dN_h = 2 \frac{km_L^{q+1}}{-q-1}, \quad (\text{for } q < -1) \quad (30)$$

the total mass m_T and the effective mass m_{eff} are, respectively, given by

$$m_T = \int_{m_0}^{m_L} m dN_h = 2 \frac{q+1}{q+2} \left[\left(\frac{m_L}{m_0} \right)^{-q-2} - 1 \right] m_L, \quad (\text{for } q \neq -2) \quad (31)$$

$$m_T m_{\text{eff}} = \int_{m_0}^{m_L} m^2 dN_h = -2 \frac{q+1}{q+3} \left[1 - \left(\frac{m_0}{m_L} \right)^{q+3} \right] m_L^2. \quad (\text{for } q \neq -3) \quad (32)$$

For $q = -2$, we have $m_T = 2m_L \ln(m_L/m_0)$.

Substituting equation (32) and the relation $m_L = 2^{1/(q+1)}m_p$ into equation (29), the condition approximately becomes

$$1 < -f_e \frac{q+1}{q+3} 2^{(q+3)/(q+1)}, \quad (33)$$

which gives $q > -2.2$ for $f_e = 1$. Since f_e is expected to be slightly smaller than unity, q would be slightly smaller than -2.2 when the largest body starts to regulate the velocity evolution. This might correspond to the value $q \simeq -2.5$ obtained by Kokubo & Ida (1996).

The fraction of planetary mass f_p is given by

$$f_p = \frac{m_p}{\int_{m_0}^{m_p} mdN_h} = \frac{q+1}{q+2} [(m_p/m_0)^{-q-2} - 1]^{-1}. \quad (34)$$

Substituting it into equation (19), we obtain the minimum oligarchic mass $m_{p,oli} = m_p(q \sim -2.2)$ as function of q . This is shown in Figure 8 as well as the corresponding m_{eff} for the parameters of Run 6. Using $m_p(q)$, we also plot the evolution of q as a function of f_p in Figure 7. As we estimated above, Figure 7 suggests that \tilde{v} starts to increase at $q \sim -2.5$ because of the gravitational scattering of planets. Therefore, when $q \sim -2.5$, growth of small planetesimals slows down as well as the evolution of their size distribution.

However, at this stage, the velocities are still not high enough to suppress the growth of large planetesimals. Therefore, mass transfer from small planetesimals to large planetesimals further increases q to ~ -2 . When $q \sim -2$, the velocity of planetesimals in the heated region is almost regulated by a single planet, whereas the contribution from a planet and all the other bodies are the same for $q \sim -2.5$. As a result, the velocity of planetesimals is enhanced toward the escape velocity of the planet. Then, actual separation of the planet from the continuous size distribution starts as we showed in § 3.1 (that is also why we keep $q = -2$ for large f_p in Fig. 7, although there is no physical reason for q to be strictly -2). Therefore, an appropriate minimum oligarchic mass to give the size distribution after the giant impact stage seems to be $m_{p,oli}$ for $q \simeq -2$ ($m_{p,oli} \sim 60m_0$ for $q = -2$ whereas $\sim 20m_0$ for $q = -2.5$). In the case of $q = -2$, $m_{p,oli}$ and m_{eff} depend on the initial planetesimal mass m_0 very weakly as $m_{p,oli}(q = -2) \propto [\ln(m_{p,oli}/m_0)]^{-3/2} \Sigma^{3/2}$ and $m_{\text{eff}}(q = -2) = 0.5m_{p,oli}(q = -2) / \ln(0.5m_{p,oli}/m_0)$.

Using the form of m_{eff} for $q = -2$, we rewire the equilibrium eccentricity (eq. [2]) as

$$e_{p,\text{eq}} = \left(\frac{2}{3} \frac{m_{p,oli}/m_0}{\ln(0.5m_{p,oli}/m_0)} \right)^{1/2} \left(\frac{m_0}{m_p} \right)^{1/6} v_{\text{esc},0}, \quad (\text{for } q = -2). \quad (35)$$

Substituting $m_{p,oli}(q = -2)$, which is obtained from eqs. [19] and [34], into eq. [35], we calculate $e_{p,eq}$ for various cases of N (or m_0) and Δ_{disk} (or Σ), assuming three final planets (thus $m_p = 0.66M_E$) and the velocity of planetesimals to be the escape velocity of a planet ($v = v_{esc,p}$).

The calculated values are plotted in Fig. 9 and compared with our N -body simulation results. We find good agreements between analytic estimates and simulations, as long as the planet-planet interactions are not important in the final state. Since the dependence of $e_{p,eq}$ on N is very weak for $N > 1000$, we need more runs for statistics. We also conducted additional simulations for the case of $N = 100$ and results are plotted in the same figure. In most of simulations with $N = 100$ (we conducted four simulations for each Δ_{disk}), giant impacts occur after nearly complete sweep up of remnant planetesimals. Therefore, it would not be appropriate to apply our analytic estimate to the case of $N = 100$. Nevertheless, we find coincidental good agreements between the averaged $e_{p,eq}$'s for simulations with $N = 100$ and those from the analytic estimates.

Finally, let us discuss what will happen if our simulations started with a very small size distribution of planetesimals. In Figure 8, we also plot $m_{p,oli}$ and m_{eff} as functions of q for the parameters used in Weidenschilling et al. (1997) ($m_0 = 4.8 \times 10^{18}g$), who conducted planetary accretion simulations in the runaway and oligarchic stages with their multi-zone code. For $(m_{p,oli}/m_0)^{-q-2} \gg 1$ (this is not the case for our simulations), the minimum oligarchic mass is given by

$$m_{p,oli} = \left(\frac{q+1}{q+2} 2\pi m_0^{-q-2} \Sigma a^2 b_p \left(\frac{2}{3M_\odot} \right)^{1/3} \right)^{-1/(q+4/3)}. \quad (36)$$

This equation indicates that $m_{p,oli}$ decreases rather strongly with m_0 for small q , as $m_{p,oli} \propto m_0^{(q+2)/(q+4/3)}$. Therefore, the minimum oligarchic mass with $q = -2.5$ for $m_0 = 4.8 \times 10^{18}g$ is much smaller than ours ($m_0 = 3.94 \times 10^{24}g$), and oligarchic bodies started to regulate the velocity evolution even when f_p is very small (estimated to be $\sim 10^{-3}$). On the other hand, $m_{p,oli}$ and m_{eff} for $q = -2$ are only one order of magnitude smaller than those for Run 6. Indeed, in simulations of Weidenschilling et al. (1997), the maximum mass of remnant planetesimals is $\sim 10^{25}g$ (whereas oligarchic bodies have masses $\sim 10^{27}g$), suggesting $q \sim -2$. Therefore, from eq. [35] the final equilibrium eccentricities is expected to be smaller than those in our simulations only by a factor of 3–4. In the discussion here, we ignored the effect of damping due to mutual collisions, which would reduce the eccentricities of planetesimals. If the fast clean up of remnant planetesimals happens due to the collisional damping, the final planetary system might be unstable, as in the case of a large g .

6. Conclusions

We have conducted direct N -body simulations of the formation of terrestrial planets beginning with a compact planetesimal disk, with the total mass and angular momentum being those for the current terrestrial planets. In most of the cases, a planetesimal disk results in three planets of similar size, and sometimes a fourth small planet forms around the location of Mars. Since a sufficient number of planetesimals remain even after giant impacts of protoplanets, orbital eccentricities of the final planets are as small as those of the current Earth and Venus. This is a very nice success of our simulations which test the standard model for planet formation.

The final eccentricities of planets are nearly in the equilibrium state for the energy partitioning with remnant planetesimals, meaning that the mutual interactions of planets in the final state is unimportant in most cases. The final eccentricities of planets depends on the initial mass of planetesimals only very weakly, and on the surface density relatively strongly. These dependences are interpreted in terms of the effective mass of remnant planetesimals ($m_{\text{eff}} = \langle m^2 \rangle / \langle m \rangle$), which determines the strength of the gravitational scattering effects of planetesimals. The mass distribution of remnant planetesimals is approximately represented by a power law distribution, $dn \propto m^q dm$, with $q \sim -2$, with the upper cut off mass (we call it the minimum oligarchic mass) which increases very weakly with the initial mass of planetesimals. Therefore, the dependence of the effective mass on the initial mass of planetesimals is very weak as well.

In a few of our simulations, planet-planet interactions are important even at the end of simulations and the orbits of final planets can be much more eccentric than for our terrestrial planets. This situation seems to appear when the gradient of population of planetesimals in the radial direction is large during the giant impact stage. However, the number of our simulations is still too small to statistically discuss the conditions that are responsible for final planetary orbits.

We appreciate an anonymous reviewer for useful comments. We are grateful to Derek Richardson for providing us with his version of *PKDGRAV*. We thank Shigeru Ida, Makiko Nagasawa, and Eiichiro Kokubo for fruitful discussions. Our simulations have been conducted with the zBox1 and zBox2 supercomputers at the University of Zurich. We thank Doug Potter for his management of the computers.

REFERENCES

- Agnor, C. B., & Ward, W. R. 2002, *ApJ*, 567, 579
- Agnor, C. B., Canup, R. M., & Levison, H. F. 1999, *Icarus*, 142, 219
- Bromley, B. C., & Kenyon, S. J. 2006, *AJ*, 131, 2737
- Chambers, J. E. 1999, *MNRAS*, 304, 793
- Chambers, J. E. 2001, *Icarus*, 152, 205
- Chambers, J. E. 2004, *E&PSL*, 223, 241
- Chambers, J. E., & Wetherill, G. W. 1998, *Icarus*, 136, 304
- Chambers, J. E., Wetherill, G. W., & Boss, A. P. 1996, *Icarus*, 119, 261
- Daisaka, J. K., Tanaka, H., & Ida, S. 2006, *Icarus*, 185, 492
- Duncan, M. J., Levison, H. F., & Lee, M. H. 1998, *AJ*, 116, 2067
- Greenberg, R., Hartman, W. K., Wacker, J., & Chapman, C. R. 1978, *Icarus*, 35, 1
- Greenzewig, Y., & Lissauer, J. J. 1992, *Icarus*, 100, 440
- Haisch, K. E., Lada, E. A., & Lada, C. J. 2001, *ApJ*, 553, L153
- Hut, P., Makino, J., & McMillan, S. 1995, *ApJ*, 443, 93
- Ida, S., & Makino, J. 1992, *Icarus*, 98, 28
- Ida, S., & Makino, J. 1993, *Icarus*, 106, 210
- Inaba, S., Tanaka, H., Nakazawa, K., Wetherill, G. W. & Kokubo, E. 2001, *Icarus*, 149, 235
- Ito, T., & Tanikawa, K. 1999, *Icarus*, 139, 336
- Iwasaki, K., & Ohtsuki, K. 2006, *AJ*, 131, 3093
- Iwasaki, K., Emori, H., Nakazawa, K., & Tanaka, H. 2002, *PASJ*, 54, 471
- Goldreich, P., Lithwick, Y., & Sari, R. 2004, *ARA&A*, 42, 549
- Kenyon, S. J., & Bromley, B. C. 2006, *AJ*, 131, 1837
- Kinoshita, H., Yoshida, H., & Nakai, H. 1991, *CeMDA*, 50, 59

- Kokubo, E., & Ida, S. 1995, *Icarus*, 114, 247
- Kokubo, E., & Ida, S. 1996, *Icarus*, 123, 180
- Kokubo, E., & Ida, S. 1998, *Icarus*, 131, 171
- Kokubo, E., & Ida, S. 2000, *Icarus*, 143, 15
- Kokubo, E., & Ida, S. 2002, *ApJ*, 581, 666
- Kokubo, E., & Makino, J. 2004, *PASJ*, 56, 861
- Kokubo, E., Kominami, J., & Ida, S. 2006, *ApJ*, 642, 1131
- Kominami, J., & Ida, S. 2002, *Icarus*, 157, 43
- Kominami, J., & Ida, S. 2004, *Icarus*, 167, 231
- Laskar, J. 1997, *A&A*, 317, L75
- Leinhardt, Z. M., & Richardson, D. C. 2005, *ApJ*, 625, 427
- Makino, J., Fukushima, T., Funato, Y., & Kokubo, E. 1998, *New A*, 3, 411
- Makino, J., Hut, P., Kaplan, M., & Saygin, H.
- Murray, C. D., & Dermott, S. F. 1999, *Solar system dynamics* (Cambridge: Cambridge Univ. Press)
- Nagasawa, M., Lin, D. N. C., & Thommes, E. W. 2005, *ApJ*, 635, 578
- Nagasawa, M., Thommes, E. W., Kenyon, S. J., Bromley, B. C., & Lin, D. N. C. 2007, in *Protostars and Planets V*, ed. Reipurth, B., Jewitt, D., & Keil, K. (Tucson: Univ. Arizona Press), 639
- O'Brien, D. P., Morbidelli, A., & Levison, H. F. 2006, *Icarus*, 184, 39
- Ogihara, M., Ida, S., & Morbidelli, A. 2007, *Icarus*, 188, 522
- Quinn, T., Tremaine, S., & Duncan, M. 1991, *AJ*, 101, 2287
- Rafikov, R. R. 2003, *AJ*, 126, 2529
- Raymond, S. N. 2005, PhD dissertation (Seattle: Univ. of Washinton)
- Raymond, S. N., Quinn, T., & Lunine, J. I. 2006, *Icarus*, 183, 265

- Richardson, D. C., Quinn, T., Stadel, J., & Lake, G. 2000, *Icarus*, 143, 45
- Saha, P., & Tremaine, S. 1992, *AJ*, 104, 1633
- Stadel, J. 2001, PhD dissertation (Seattle: Univ. of Washington)
- Yoshinaga, K., Kokubo, E., & Makino, J. 1999, *Icarus*, 139, 328
- Youdin, A. N., & Shu, F. H. 2002, *ApJ*, 580, 494
- Weidenschilling, S. J., Spaute, D., Davis, D. R., Marzari, F., & Ohtsuki, K. 1997, *Icarus*, 128, 429
- Wetherill, G. W., & Stewart, G. R. 1989, *Icarus*, 77, 330
- Wetherill, G. W., & Stewart, G. R. 1993, *Icarus*, 106, 190
- Wisdom, J., & Holman, M. 1991, *AJ*, 102, 1528

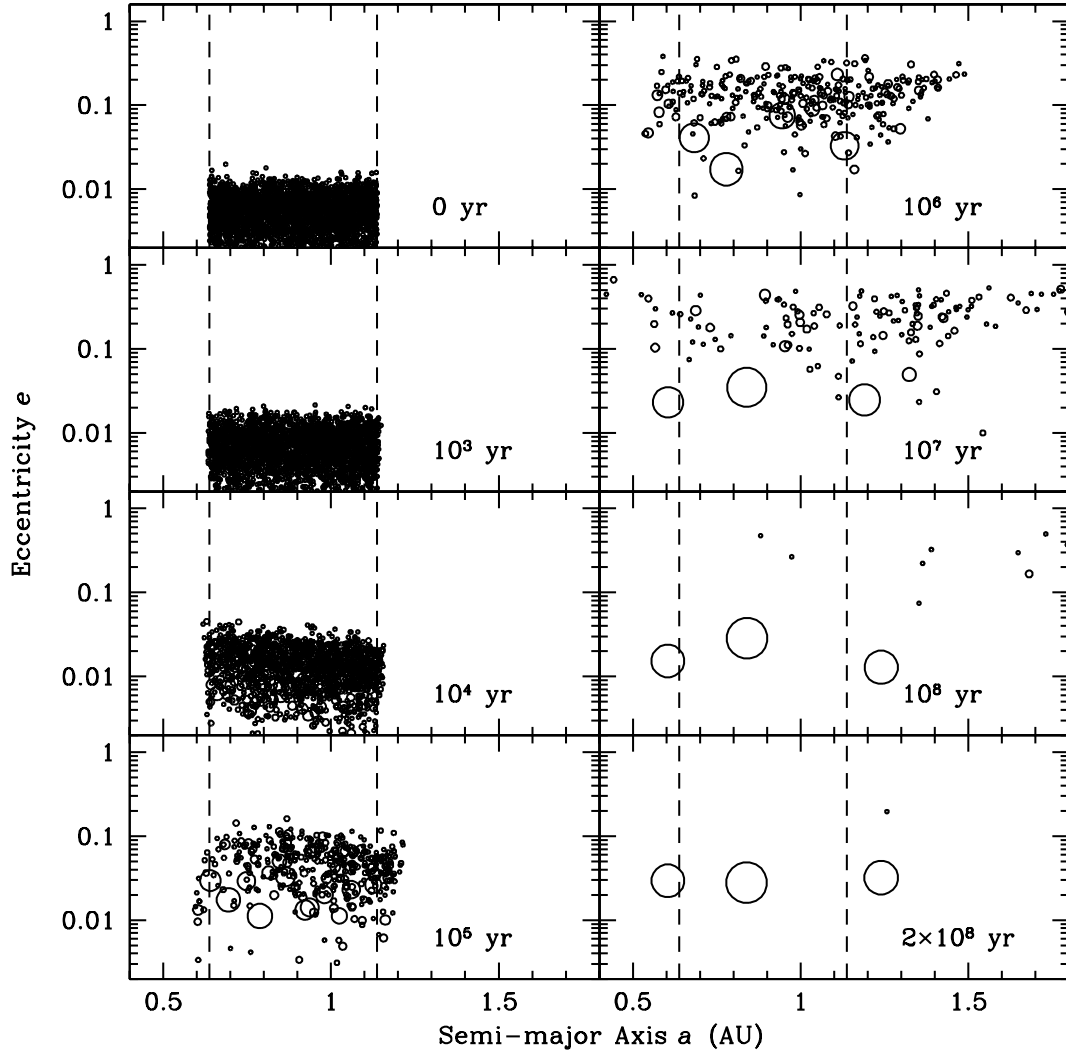


Fig. 1.— Snapshots of Run 6 on the a - e plane. Vertical dashed lines are the inner and outer edges of the initial planetesimal disk. The circles represent planetesimals and planets, and plotted radius sizes are proportional to the actual radii without artificial enhancement.

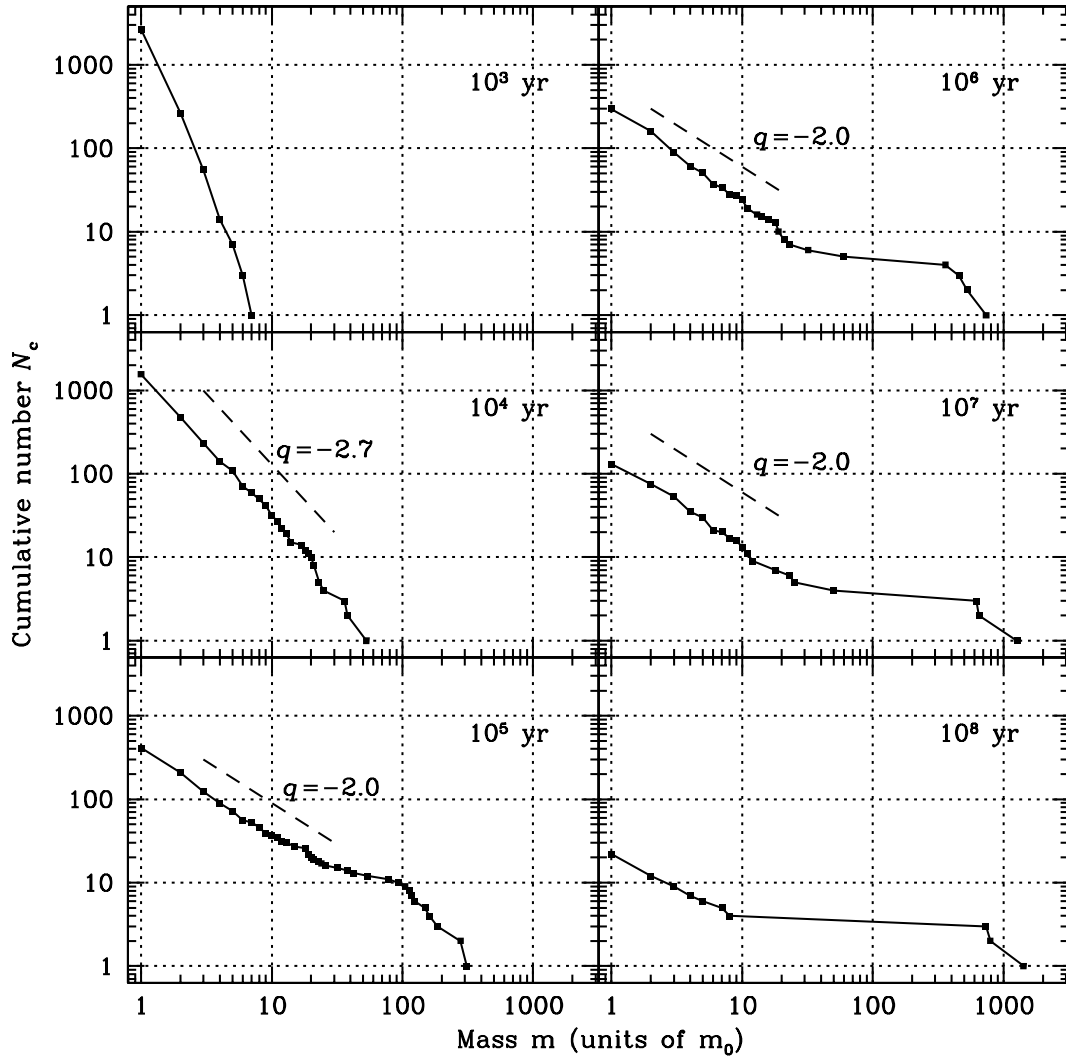


Fig. 2.— Evolution of the cumulative number vs. mass in units of the initial mass for Run 6. The slope of the approximated power-law distribution, $dN_c \propto m^q dm$, is shown in each panel.

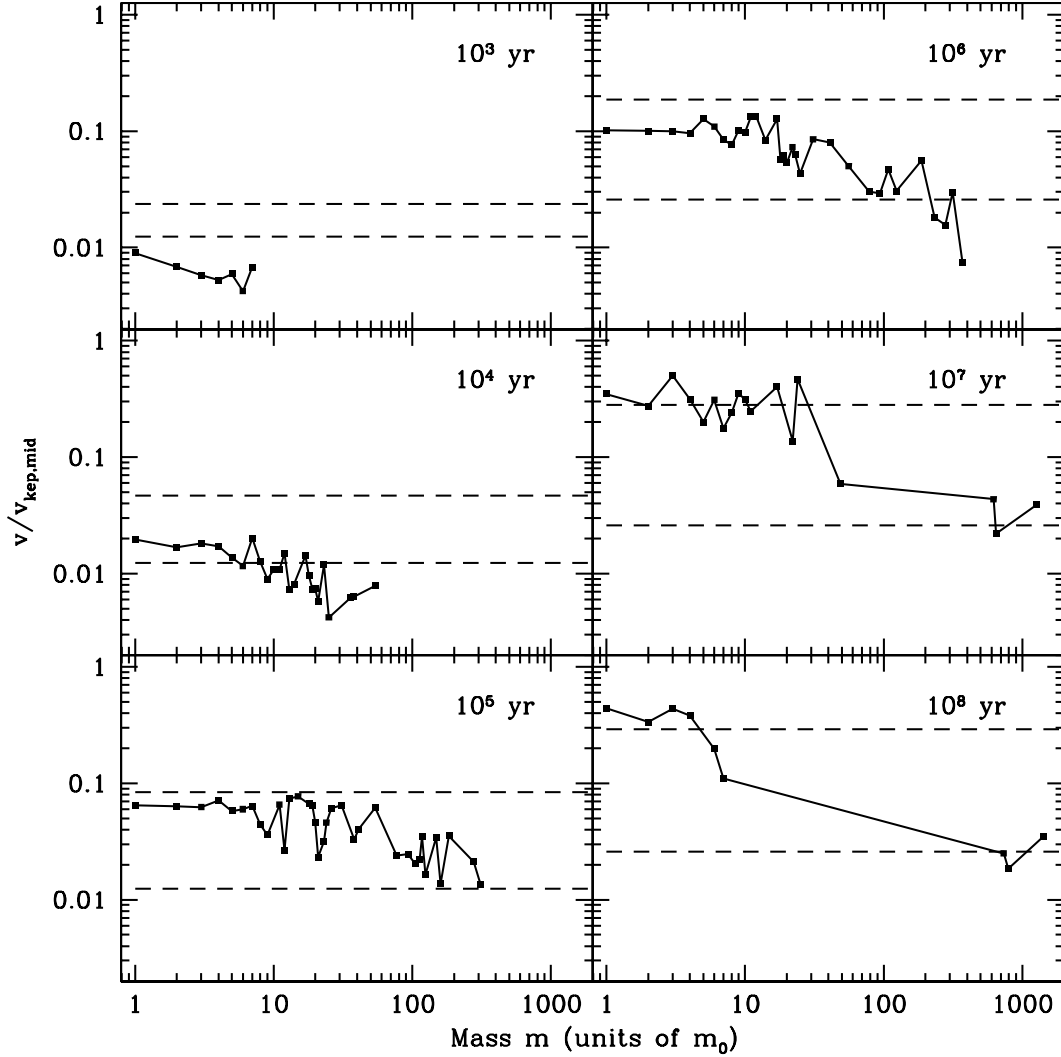


Fig. 3.— Evolution of the epicyclic velocity vs. mass for Run 6. The velocity is normalized by the Keplerian velocity $v_{\text{kep,mid}}$ at $a = 0.89\text{AU}$. The upper and lower horizontal dashed lines represent the escape velocities of the largest body and the smallest body, respectively. Note that the escape velocity of the smallest body increases by a factor of \sqrt{g} after 10^5 years as we reduce the radius enhancement factor g from 4.3 to 1.

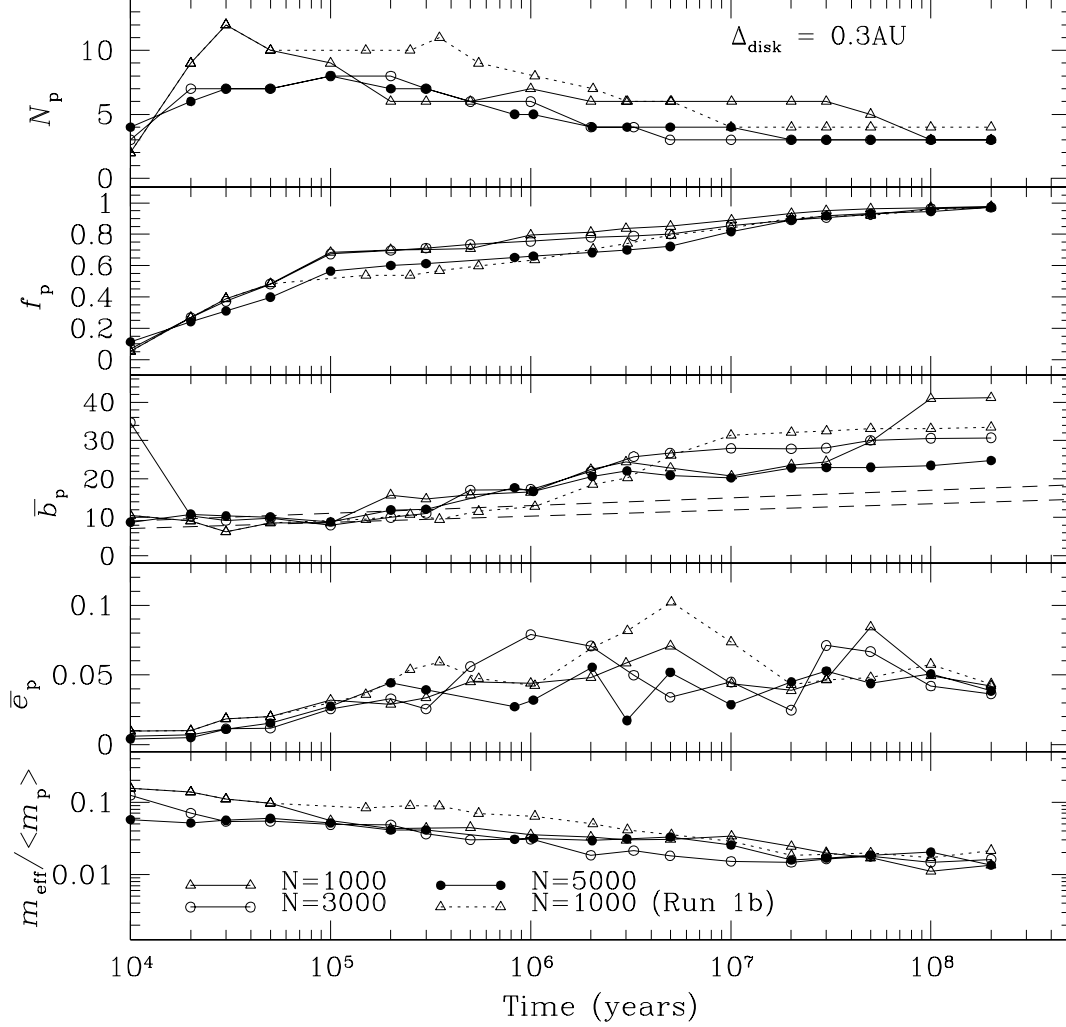


Fig. 4.— Time evolution of the averaged quantities for $\Delta_{\text{disk}} = 0.3\text{AU}$ (Runs 1, 1b, 2, and 3). From top to bottom, the panels show the number, mass fraction, orbital spacing, and orbital eccentricity of planets ($m > 2 \times 10^{26}$ g), and the ratio of the effective mass of planetesimals to the mean mass of planets. In the third panel, the relations between the orbital spacing and orbital instability time for $\bar{e}_p/\bar{h}_p = 2$ and 4 (Yoshinaga et al. 1999) are shown by lower and upper dashed lines, respectively.

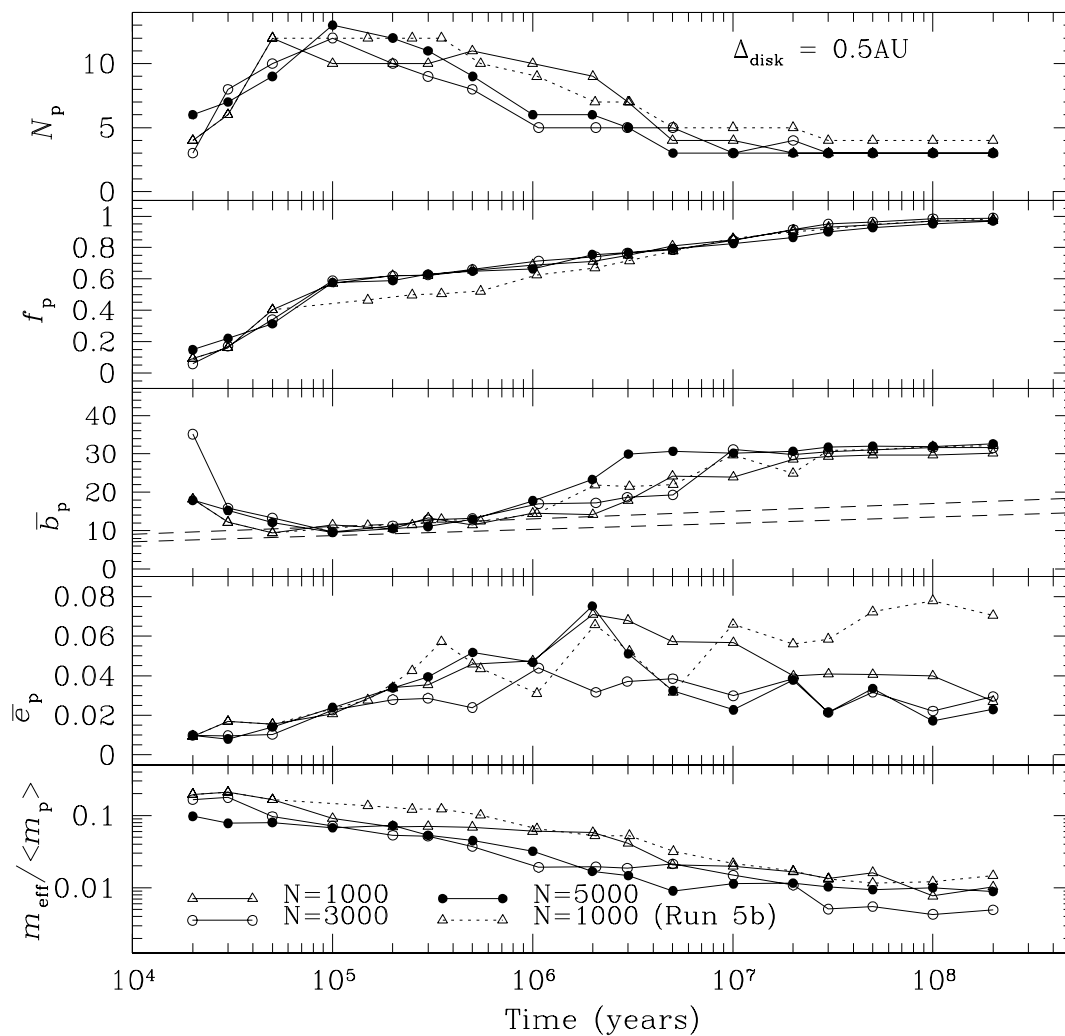


Fig. 5.— Same as Figure 4 but for the case of $\Delta_{\text{disk}} = 0.5\text{AU}$ (Runs 5, 5b, 6, and 7).

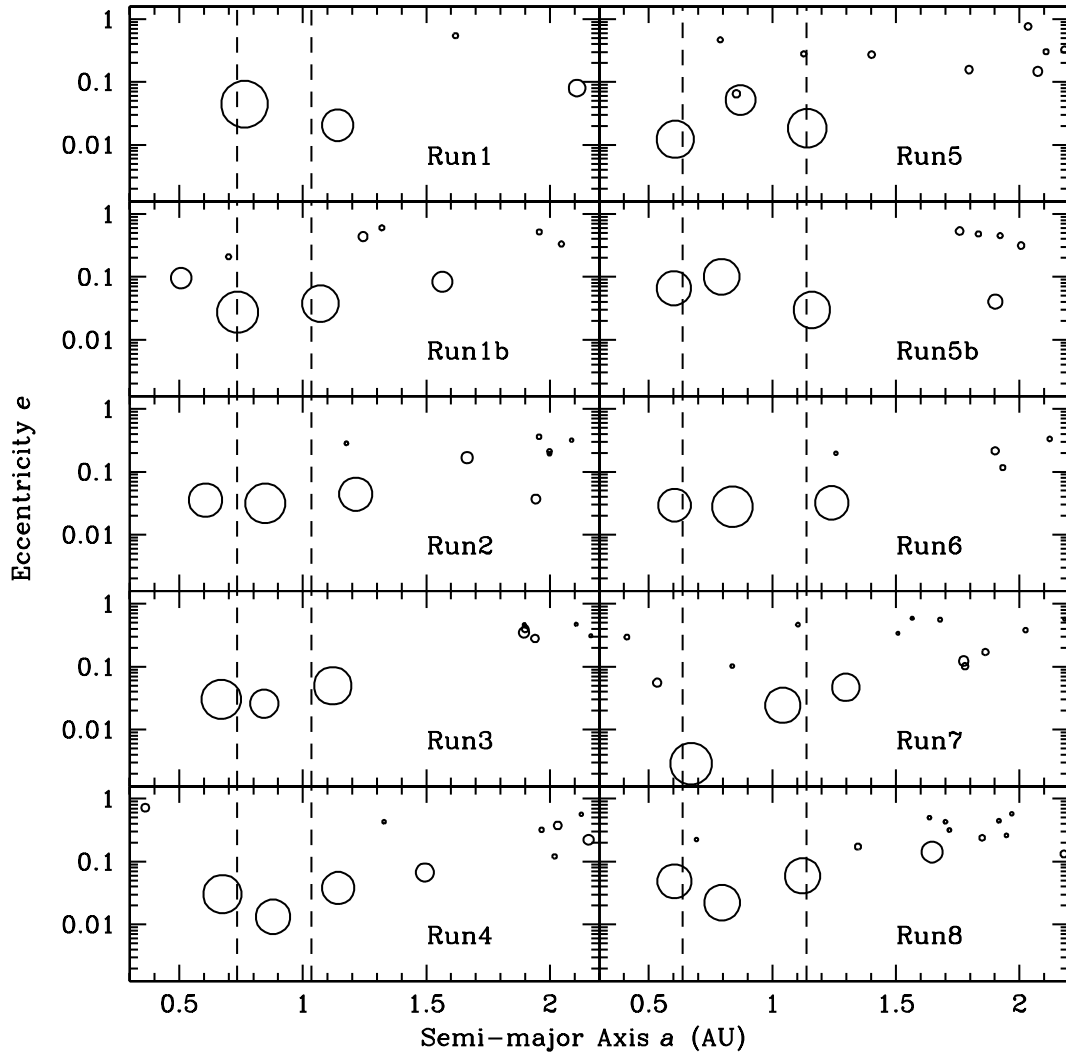


Fig. 6.— Snapshot of all of runs on the a - e plane at 200Myr. The vertical lines represents inner and outer edges of the initial planetesimal disk.

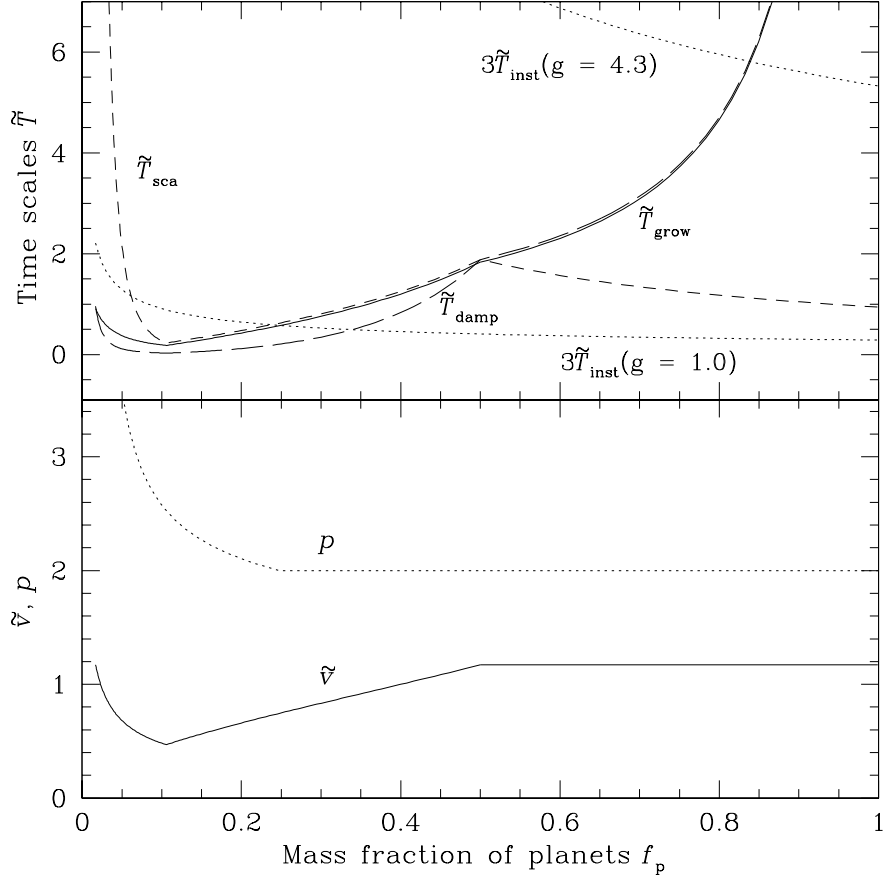


Fig. 7.— Evolution of the normalized time scales \tilde{T} (upper panel), the velocity of planetesimals \tilde{v} normalized by the escape velocity of planets, and the power-law index, q , for mass distribution of planetesimals (lower panel) as functions of mass fraction of planets f_p to the total mass. \tilde{T}_{grow} , \tilde{T}_{scat} , \tilde{T}_{damp} , and $\tilde{T}_{\text{inst}}(g)$ represent time scales for the growth of planets, evolution of the planetesimal velocity due to scattering by planets, damping of eccentricities of planets due to the dynamical friction of planetesimals, and orbital instability for multiple planet systems, respectively. \tilde{T}_{grow} is slightly shifted downward (by 0.05) to avoid overlapped displays of the time scales.

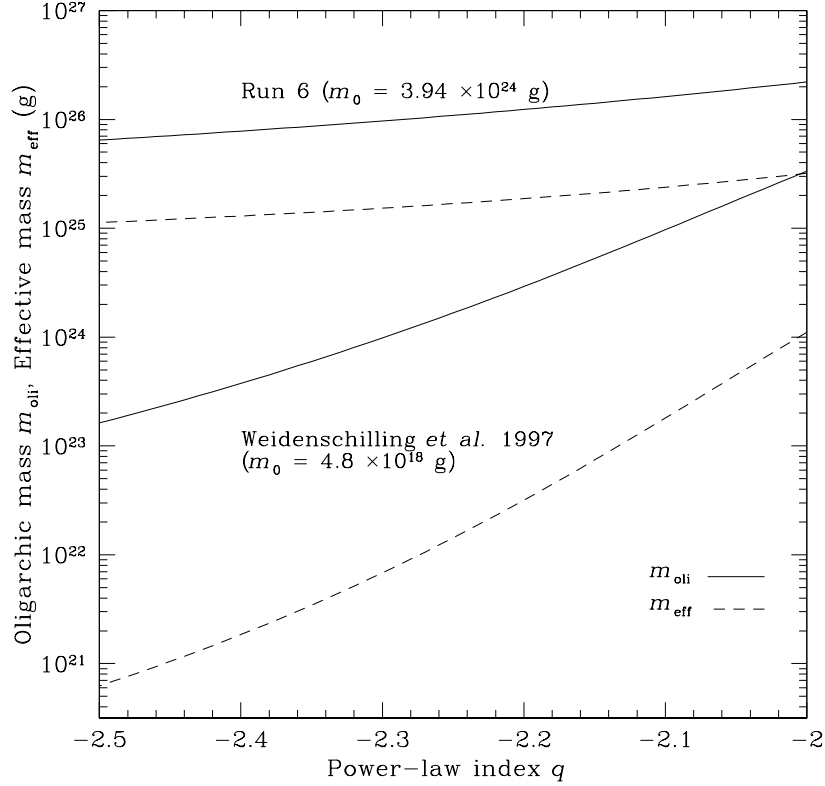


Fig. 8.— The minimum oligarchic mass $m_{p,oli}$ (solid lines) and the effective mass of planetesimals m_{eff} (dashed lines) versus the power-law index q . The case for our Run 6 ($m_0 = 3.94 \times 10^{24}$ g, $\Sigma = 19.1$ g cm $^{-2}$, and $a = 0.89$ AU), and the case for parameters used in simulations of Weidenschilling *et al.* (1997) ($m_0 = 4.8 \times 10^{18}$ g, $\Sigma = 16.7$ g cm $^{-2}$, and $a = 1.0$ AU) are shown. The latter parameters are also used in Wetherill & Stewart (1993) and Inaba *et al.* (2001).

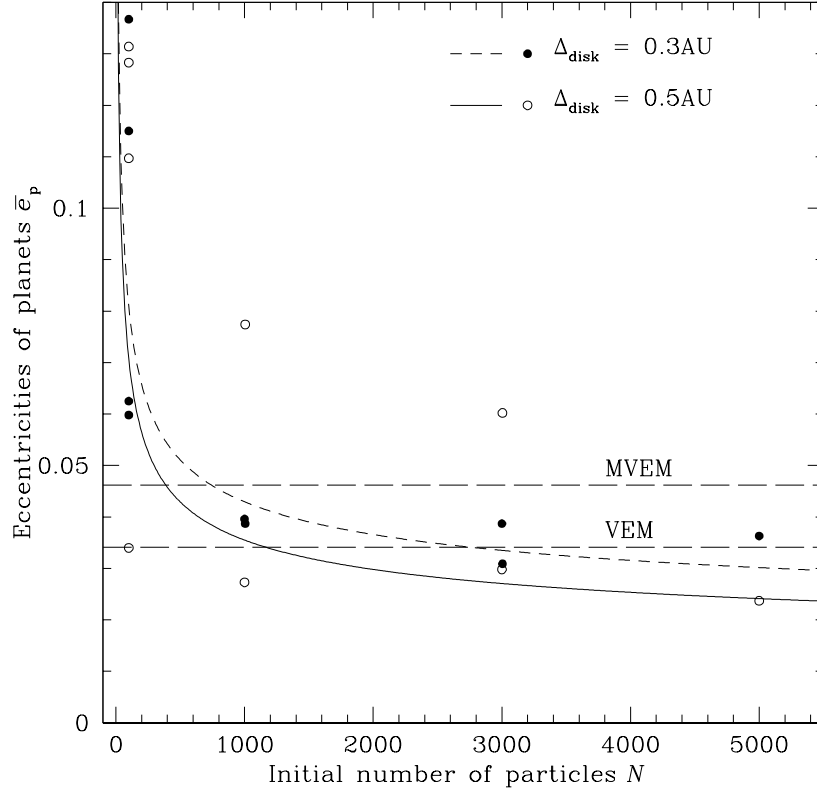


Fig. 9.— Comparison of the final eccentricities of planets between N -body simulations (open and filled circles; from Table 1 except for $N = 100$) and analytic estimates (solid and dashed lines; eq. [35]). In analytic estimates, we assume the mass of planets m_p to be $0.66M_E$ and $q = -2$ for remnant planetesimals. MVEM and VEM stand for the values for the current terrestrial planets with and without Mercury, respectively.

Table 1. Initial conditions and final states of simulations

Run	$\Delta_{\text{disk}}(\text{AU})$	N	α	N_{p}	$\bar{e}_{\text{p}} (10^{-2})$	$S_{\text{d}} (10^{-3})$
1	0.3	1000	-1	3	3.96	1.55
1b	0.3	1000	-1	4	3.87	1.51
2	0.3	3000	-1	3	3.87	1.79
3	0.3	5000	-1	3	3.63	0.99
4	0.3	3000	-2	4	3.09	0.99
5	0.5	1000	-1	3	2.73	0.95
5b	0.5	1000	-1	4	7.74	3.49
6	0.5	3000	-1	3	2.98	0.60
7	0.5	5000	-1	3	2.37	0.49
8	0.5	3000	-2	4	6.02	2.97
MVEM				4	4.62	1.90
VEM				3	3.41	1.50

Note. — Parameters Δ_{disk} , N , and α stand for the width, number of planetesimals, and power-law index for the surface density of initial planetesimal disks, respectively, and N_{p} , \bar{e}_{p} , and S_{d} stand for the number, averaged orbital eccentricity (eq. [3]), and angular momentum deficit of planets (eq. [8]) at the end of simulations. In Runs 1b and 5b we switch integrators and reduce g to unity at 5×10^4 yr, and at 10^5 yr for other runs. MVEM and VEM stand for the current terrestrial planets with and without Mercury, respectively.